Faraday Discussions

Accepted Manuscript

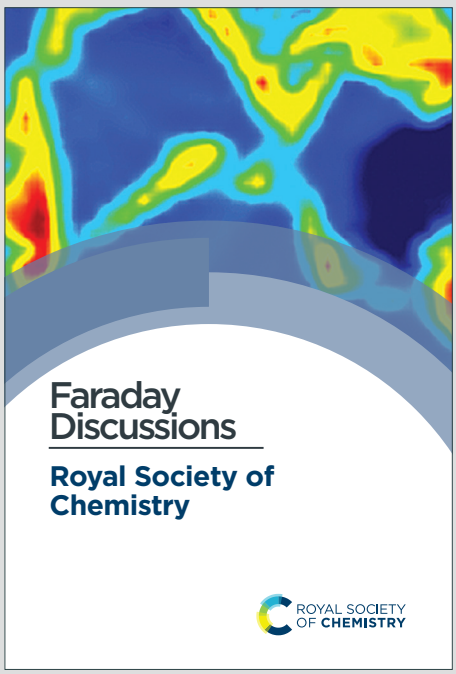

This article can be cited before page numbers have been issued, to do this please use: G. Gurieva, K. Ernits, D. Sheptyakov, A. Manjón-Sanz, M. J. Kirkham, M. Avdeev, N. Siminel, D. Meissner and S. Schorr, *Faraday Discuss.*, 2026, DOI: 10.1039/D6FD00010J.

Atomic structure and structural disorder vs. device efficiency in Kesterite monograin solar cells with S/(S+Se)≈0.8

View Article Online
DOI: 10.1039/D6FD00010J

G. Gurieva[1], K. Ernits[2], D. Sheptyakov [3], A. Manjon Sanz [4], M. Kirkham[4], M. Avdeev[5], N. Siminel[6], D. Meissner[2,7], S. Schorr[1,8]

[1] Helmholtz-Zentrum Berlin für Materialien und Energie, Berlin,Germany
[2] Crystalsol OÜ, Tallinn, Estonia
[3] Laboratory for Neutron Scattering and Imaging, Paul Scherrer Institut, Villigen, Switzerland
[4] Neutrons Scattering Division, Oak Ridge National Lab, Oak Ridge, Tennessee, United States
[5] Australian Nuclear Science and Technology Organisation, Lucas Heights NSW, Australia
[6] Institute of Applied Physics, Academy of Sciences of Moldova, Chisinau, Moldova
[7] Department of Materials and Environmental Technology, Tallinn University of Technology, Tallinn, Estonia
[8] Freie Universität Berlin, Institute of Geological Sciences, Berlin, Germany

Abstract

Cu-poor/Zn-rich $Cu_2ZnSn(S,Se)_4$ (CZTSSe) monograins with S/(S+Se) = 0.8 were investigated using neutron powder diffraction to directly quantify Cu/Zn disorder and intrinsic point defects. According to their chemical composition, the monograins show a mixture of the off-stoichiometry types A and B. Monograins with a predominantly A-type off-stoichiometry exhibit reduced Cu/Zn disorder and increased V_{Cu} concentrations, whereas Zn_{Sn} defect concentration increases with increasing B-type off-stoichiometry. Zn_{Cu} antisite defects, belonging to both A and B off-stoichiometry types increase with increasing deviation from stoichiometry, and the combined defect concentration is lowest towards the stoichiometric point and A-type line, correlating with highest photovoltaic efficiency. Opposing trends are observed between optical band gap and solar cell stability, indicating that monograin solar cells with the same anion ratio but lower band gap energy are more stable. By correlating the atomic-scale defect scenario to macroscopic device performance, these results provide a quantitative framework for defect engineering in kesterite-type absorbers.

Introduction

Quaternary chalcogenides, especially kesterite-type $Cu_2ZnSn(S,Se)_4$ (CZTSSe), have attracted considerable attention as emerging absorber materials for photovoltaic (PV) applications. PV devices based on off-stoichiometric CZTSSe absorber layers [1] have achieved power conversion efficiencies of up to 16.5% [2]. Due to the non-toxicity and abundance of their constituent elements, CZTSSe compound semiconductors represent a promising low-cost alternative absorber for thin-film solar cells that are free of critical raw materials.

Deviations from stoichiometry in CZTSSe are possible due to the flexibility of the kesterite-type structure to accept intrinsic point defects (vacancies, anti-sites, interstitials) [3]. These point defects, occurring in high concentrations up to 10^{20} cm^{-3}, can be discussed as the materials' structural disorder. A special kind of this disorder is the Cu/Zn disorder (Cu_{Zn} and Zn_{Cu} anti-sites on distinct structural Cu and Zn sites) is always present in kesterite-type compounds [4, 5]. The formation of intrinsic point defects is creating energy levels within the band gap, thereby influencing charge carrier concentrations, conductivity, optical properties, recombination dynamics, and ultimately device performance limits [6]. Thus, knowledge about intrinsic point defect scenarios and control of defect processes in PV materials is essential for realizing high-efficiency solar cells and related optoelectronic devices.

The determination of the cation distribution on the four structural cation sites of the kesterite-type structure, especially with respect to Cu^+ and Zn^{2+} has been approached in various ways [7], deducing indirectly the decrease of Cu/Zn disorder at temperatures below the order-disorder transition temperature: by anomalous lattice parameter expansion [8], Raman spectroscopy and

View Article Online
DOI: 10.1039/D6FD00010J

spectrophotometry [9], electro-reflectance [10], and from kinetics simulations [11]. Despite these efforts, a substantial gap remains between such studies and a fundamental understanding of Cu/Zn disorder in CZTSSe, as most of these studies are performed on thin films, by methods which can provide access to the Cu/Zn disorder only indirectly. Polycrystalline thin film absorber layers are usually inhomogeneous, with an off-stoichiometric absorber composition and often containing secondary phases [3]. Separating Cu_{Zn} and Zn_{Cu} anti-site point defects causing Cu/Zn disorder from the other intrinsic point defects correlated to the off-stoichiometric absorber composition (i.e. to the off-stoichiometry type related point defects) is a very complex problem [5]. In order to determine Cu/Zn disorder in a direct approach and even more to quantify the level of disorder by an order parameter, it is necessary to locate the positions of Cu^{+} and Zn^{2+} within the kesterite-type structure. The most efficient solar cells tend to have off-stoichiometric composition, and be located in the A-B off-stoichiometry type region, corresponding to the Cu-poor/Zn-rich composition, and the defect complexes V_{Cu}+Zn_{Cu} (A-type), $2Zn_{Cu}$+Zn_{Sn} (B-type) [5]. We have developed a methodology to determine the type and concentration of intrinsic point defects from diffraction data [12].

Here we applied neutron diffraction, which enables reliable discrimination between the isoelectronic elements copper and zinc in the structural analysis. On the other hand, neutron diffraction requires large sample volumes. In the present study we have investigated CZTSSe monograins (single crystals of 50-100 µm size) by neutron powder diffraction, which are later fixed in a polymer matrix to form a flexible solar cell [13, 14]. The monograin approach gained a lot of attention lately, for solar module production, providing a third alternative to mono-crystalline wafer and thin film methods [15]. The monograin membrane approach combines the advantages of high throughput, low-cost deposition techniques primarily from the printing industry with the versatility of a flexible, lightweight, thin film solar module. In general, powder-based technologies are the least expensive methods of creating materials [13, 16]. A comparison of monograin and thin film production demonstrated that monograin can outperform the thin film technology in some cases and was proximate to CIGS ($Cu(In,Ga)Se_2$) even considering their higher achieved efficiency [17]. The life cycle analysis presented considerable environmental benefits associated with the monograin technology [17].

In our case kesterite monograins offer the unique possibility to directly correlate structural disorder in kesterite-type absorbers with device performance parameters of the monograin layer solar cell [18]. While related studies have previously addressed the understanding of the influence of the mechanical and thermal treatments [18] as well as the purity of the elements used in synthesis [19], the focus here is on a detailed structural investigation of a Cu-poor/Zn-rich CZTSSe monograins with S/(S+Se)=0.8 based on neutron powder diffraction experiments, examining the influence of changes in the off-stoichiometric composition on the Cu/Zn disorder and the intrinsic point defect scenario as well as the optical bandgap and finally the device performance parameters. By directly linking atomic-scale structural features to macroscopic device characteristics, this work provides a foundation for defect engineering in kesterite-type PV absorber materials.

Experimental

The twenty-seven CZTSSe monograin samples used in this work were grown following the standard monograin technology used at Crystalsol OÜ described previously in detail [13, 14]. This set of samples was also part of a previously published study [20], looking into stability (performance in the solar cells after 1000 hours at 80 C in dry heat, e.g. if the efficiency after the test did not change – stability equals to 1, if the efficiency after 1000 hours at 80 C in dry heat is decreased with 50%, the stability value is 0.5), reliability, upscaling and possible technological applications of Kesterite solar cells (the previously

View Article Online
DOI: 10.1039/D6FD00010J

published data are the values for efficiency and stability). These particular CZTSSe samples were grown aiming for a S/(S+Se) ratio of 0.8 and an A-B type off-stoichiometry [5], Cu-poor and Zn-rich, which is typically referred as the best off-stoichiometry region for CZTSSe solar cells [13].

To determine the chemical composition and phase content of the samples, wavelength dispersive X-ray spectroscopy (WDX) has been performed using an electron microprobe analysis system (JEOL-JXA 8200) equipped with a wavelength dispersive X-ray spectroscopy unit (WDX) in the same way as in our previous studies of CZTSSe monograins, the details can be found in [18, 19]. As a result, it turned out that 8 out of 27 monograins show signs of inhomogeneity, and were excluded from the further study at this step. All of the homogeneous monograins are placed in the Cu-poor, Zn-rich quadrant of the cation ratio plot (Figure 1), but not all of them ended up in the intended A-B off-stoichiometry region. Some spill overs in the A – L and B – G off-stoichiometry regions were detected. According to our previous studies [5], the defect complexes we could expect in accordance to the off-stoichiometry type in the homogeneous monograins are V_{Cu}+Zn_{Cu} (A-type), 2Zn_{Cu}+Zn_{Sn} (B-type), Zn_{Sn}+Zn_i (G-type) and 4V_{Cu}+Zn_{Cu}+ Sn_{Cu} (L-type). Small amounts of ZnS or $ZnS_{0.9}Se_{0.1}$ as secondary phase were detected in some of the samples. The complete overview of the obtained cation ratios and deducted chemical composition of all of the homogeneous CZTSSe monograins is shown in Table 1.

The structural characterization of the 19 homogeneous monograins was performed using neutron diffraction (NPD). Neutron diffraction experiments have been performed at three different sources: a) at the Swiss Spallation Neutron Source (SINQ) at the Paul-Scherrer Institute (PSI) using the High-Resolution Powder Diffractometer for Thermal Neutrons (HRPT) (λ=1.1545 Å, ambient temperature) [21, 22] (ID 20202094); b) at the Spallation Neutron Source (SNS, Oak Ridge National Laboratory) using the POWGEN BL-11A powder diffractometer [23] (IPTS 26264) at room temperature, a center wavelength of 1.5 Å was used, covering a *d*-spacing range of 0.485-13 Å; c) Echidna, the High-Resolution Powder Diffractometer at the Australian Centre for Neutron Scattering (ACNS) at ANSTO [24], at room temperature using neutrons with a wavelength λ = 1.6215 Å within a 2θ range from 10 to 165° (ID P9796). The collected datasets were then analyzed by full pattern Rietveld refinement [25] using the FullProf Suite software package [26]. The kesterite type structure (space group $I\bar{4}$) with Cu on Wyckoff positions 2*a*:(0,0,0) and 2*c*:(0,½,¼), Zn on 2*d*:(0, ½,¾), Sn on 2*b*:(½, ½,0) and S and Se on 8*g*:(*x*,*y*,*z*) was used as structural model in the refinement [27]. The refinement of site occupancy factors (SOF) was done without any chemical constraints (Table 2). An example of neutron diffraction pattern measured at HRPT and the corresponding Rietveld analysis of the data for $Cu_{1.98}Zn_{1.04}Sn_{0.99}S_{3.26}Se_{0.74}$ is shown in Figure 2 left. The average neutron scattering length analysis method [12] was applied to determine the distribution of the cations Cu^+, Zn^{2+} and Sn^{4+} on the four structural sites of the kesterite type structure (2*a*, 2*b*, 2*c* and 2*d*). The experimental average neutron scattering lengths (*b*) were calculated according to Eqs. 1 using the cation site occupancy values SOF_{2a}, SOF_{2c}, SOF_{2d} and SOF_{2b} determined by Rietveld analysis of neutron diffraction data:

$$\begin{aligned} \bar{b}_{2a}(exp) &= SOF_{2a} \cdot b_{Cu} \\ \bar{b}_{2c}(exp) &= SOF_{2c} \cdot b_{Cu} \\ \bar{b}_{2b}(exp) &= SOF_{2d} \cdot b_{Zn} \\ \bar{b}_{2b}(exp) &= SOF_{2b} \cdot b_{Sn} \end{aligned} \qquad (1)$$

The corresponding average neutron scattering length analysis for the $Cu_{1.98}Zn_{1.04}Sn_{0.99}S_{3.26}Se_{0.74}$ is presented in Figure 2 (right). The details of the cation distribution model, which is introduced for each of the monograins can be found in [5]. It is important that the sum of a cation species on the different

View Article Online
DOI: 10.1039/D6FD00010J

cation sites should be in good agreement with the chemical composition of the phase determined by WDX analysis. In the case of an excess of a cation species, e.g. the sum of a cation species distributed at the cation sites is less than the amount determined by WDX, interstitials are assumed. Considering the experimentally determined total amounts of each element, as obtained by WDX analysis, and assuming that all four cation sites are fully occupied, the respective cation occupancy of the sites can be derived with high reliability.

Diffuse Reflectance Spectroscopy (DRS) measurements were carried out in air at room temperature in a spectrophotometer equipped with an integrating sphere - Perkin Elmer UV/Vis-spectrometer Lambda 750S. The measurement range was adjusted for this set of samples - 1000 – 1400 nm with a step size of 1nm. Tauc plots were obtained by plotting $(F(R)*h\nu)^2$ versus the photon energy [28]. The linear part of the curve was extrapolated to the baseline, and the optical band gap was extracted from the value of intersection.

Results and discussion

The average scattering length analysis for the $Cu_{1.98}Zn_{1.04}Sn_{0.99}S_{3.26}Se_{0.74}$ monograin, showing an A-B type off-stoichiometry is shown in Figure 2 (right). It can be observed that the experimental average neutron scattering lengths of the positions 2*c* and 2*d* significantly deviate from values expected on these sites according to the kesterite type structure (b_{Cu}=7.718 fm and b_{Zn}=5.680 fm). The experimental value for the 2*c* site is significantly lower, and the one for 2*d* is significantly higher than the expected neutron scattering length on these sites. Such scattering length differences can be explained by the formation of intrinsic point defects. For instance, zinc on copper anti-site defects (Zn_{Cu}) would decrease the average neutron scattering length of the 2*c* crystallographic site because b_{Zn}=5.680 fm< b_{Cu}=7.718 fm, likewise the copper on zinc anti-site defect (Cu_{Zn}) would lead to an increase of the average neutron scattering length of the 2*d* site in this way forming the Cu/Zn disorder. The very slightly lower than expected value of the experimental average neutron scattering length at the 2*a* site is mainly due to copper vacanvies (V_{Cu}) and Zn_{Cu} anti-sites. The formation of Zn_{Sn} anti-site is responsible for a slightly lower than expected value at the 2*b* site. The experimentally determined concentration of these point defects is summarized in Table 3.

Using the site occupancy factors the order parameter *Q* of the Cu/Zn disorder can be calculated. This order parameter is defined in such a way that *Q* = 0 for complete disorder (Cu and Zn are distributed randomly on the Wyckoff sites 2c and 2d) and *Q* = 1 for order (Cu on the Wyckhoff site 2*c* and Zn on the site 2*d*). In literature different approaches can be found [7, 29] depending on whether the copper site 2*a* is included and how vacancies are treated. For the kesterite-type CZTSSe phases studied here the approach discussed in [7] was used, the same way as for stoichiometric CZTSSe powders in [29]. Thus eq.2 was adapted from [7]:

$$Q = \frac{[Cu_{2c}+Zn_{2d}]-[Zn_{2c}+Cu_{2d}]}{[Cu_{2c}+Zn_{2d}]+[Zn_{2c}+Cu_{2d}]}. \quad (2)$$

This type of analysis was performed for all of the monograins studied by neutron diffraction, thus it was possible to map the Q value on the cation ratio plot (Figure 3). The lower the Q value, the higher the Cu/Zn disorder, and the higher the Q value the lower the Cu/Zn disorder. It can be clearly seen that there are a few areas on the map where the Q values are the highest, pointing towards low Cu/Zn disorder. Those areas are all located within the A-B off-stoichiometry type segment of the cation ratio plot, with the first one pointing at the closest to the stoichiometry point compositions in the area, and the other two being more off-stoichiometric, and grouping either close to the B-type line or in the middle of the A-B area.

View Article Online
DOI: 10.1039/D6FD00010J

Similarly, the off-stoichiometry type related intrinsic point defects were mapped on the cation ratio plot (Figure 4). According to the classification introduced in [30], all of the off-stoichiometry related defects based on their potential influence on the performance of the CZTSSe absorbers can be divided in so-called "good" (e.g. giving rise to conductivity), "not favorable" (e.g. electrically inactive) and "bad" (e.g. deep states in the electronic bandgap which may act as non-radiative recombination centers). The A-type defects are a combination of V_{Cu} "good" defect with Zn_{Cu} "not favourable" defect, while the B-type defects are a combination of Zn_{Cu} "not favourable" defect with Zn_{Sn} mid gap defect ("bad" defect). This type of classification is also reflected in the colour scheme of the Figures 4. The additional defect types for the L- and G-types are Sn_{Cu} mid gap defect and Zn_i respectively, both being "bad" defects. The number of monograins in those areas was not enough to produce any meaningful map for these defects, but the values are presented in Table 3. As expected, the highest concentration of "good" V_{Cu} can be found close to A-type line. At the same time the "not favourable" Zn_{Cu} defect, present in both A and B off-stoichiometry types, has the lowest concentration towards the stoichiometry point (Figure 4). The concentration of the B-type related Zn_{Sn} "bad" mid gap defect is increasing towards the B-type line. In order to get a better understanding of the general off-stoichiometry related defect type scenario, we calculated the total concentration of these defects, which is presented in Figure 4 bottom right. The lowest total defect concentration can be found between the A- and B- type lines, towards the stoichiometry point. This area to a degree overlaps with one of the highest Q (lowest Cu-Zn disorder) areas (Figure 3), making it the most promising one for the potential applications from the structural disorder point of view (both Cu/Zn disorder and off-stoichiometry related intrinsic point defects).

In order to have a better understanding of the correlation of the structural findings with the device efficiency in kesterite monograin solar cells with S/(S+Se)≈0.8, we concentrated on three parameters – band gap energy, solar cell efficiency and stability [13] (Table 4, Figure 5). These parameters were mapped on the cation ratio plot in the same way as the defects. The trend we notice in the band gap energy is similar to the one in Cu/Zn disorder, meaning that CZTSSe monograins with the same, or very similar anion ratios have relatively lower band gap in areas where the Cu/Zn disorder is higher. We already noticed a similar trend earlier, but in a smaller sample set [19], this is also in a good agreement with the calculations made for CZTS in [30]. The noticeable trend in the efficiency values points toward its increase towards A-type off-stoichiometry line and stoichiometry point in solar cells based on the CZTSSe monograins. Opposite trends in stability and E_g (optical band gap) were found, highlighting that CZTSSe monograins with the same, or very similar anion ratios with relatively lower bandgap (the small differences are due to Cu/Zn disorder and off-stoichiometry in this case) are more stable. Summarizing all of the above, the compositional area closer to the A-type off stoichiometry line, while still close to the stoichiometry point, should be the most beneficial for the kesterite monograin solar cells with S/(S+Se)≈0.8

Conclusion

Our systematic study of CZTSSe monograins revealed correlations between their atomic-scale point defect scenario and the macroscopic performance of the respective PV device. Our findings are based on in-depth investigation of CZTSSe monograins (with S/(S+Se)=0.8) chemical composition, Cu/Zn disorder, intrinsic point defects, band gap energy and stability. It was found that CZTSSe monograins with a composition closer to the off-stoichiometry A-type line have lower Cu/Zn disorder. The concentrations of the intrinsic point defects specific to only one of the off-stoichiometry types is increasing in the phases with the compositions closer to the corresponding types: the defect

concentration of V_{Cu} is increasing closer to the A-type and the concentration of the Zn_{Sn} defect is increasing closer to the B-type line respectively. The situation changes for the defect present in both off-stoichiometry types: the defect concentration of the Zn_{Cu} is increasing from the stoichiometric point outwards, i. e. with increasing off-stoichiometry. A map of the sum of all this defect's concentrations shows a minimum in the area closest to the stoichiometry point and A-type line. Additionally, opposite trends in stability and optical band gap were found. That means that the corresponding solar cells based on CZTSSe monograins with the same, or very similar anion ratios with relatively lower bandgap are more stable. The power conversion efficiency of the respective solar cell shows a trend similar to the sum of the defect concentrations; it increases towards A-type line and stoichiometry point, where the defect concentration decreases. Taken together, our results highlight off-stoichiometry engineering as a key lever for controlling point defects in CZTSSe monograins and for optimizing both the stability and performance of the resulting photovoltaic devices.

Acknowledgements:

This work is partly based on experiments performed at the Swiss SNS SINQ (experiment no. 20202094), from the Paul Scherrer Institut. A portion of this research used resources at the Spallation Neutron Source, a DOE Office of Science User Facility operated by the Oak Ridge National Laboratory (IPTS-26264 for POWGEN experiment). We thank the Australian Nuclear Science and Technology Organization (ANSTO), Sydney, for access to the powder neutron diffraction facility (Echidna), proposal ID: P9796. The research leading to the presented results has been partially supported by the CUSTOM-ART Project. This project received funding from the European Union's Horizon 2020 Research and Innovation Programme under the Marie Skłodowska-Curie Grant (Agreement No. 952982).

Data availability statement

The data cannot be made publicly available upon publication because the cost of preparing, depositing and hosting the data would be prohibitive within the terms of this research project. The data that support the findings of this study are available upon reasonable request from the authors.

References

1. Zhou J., Xu X., Duan B., Wu H., Shi J., Luo Y., Li D., Meng Q., *Regulating crystal growth via organic lithium salt additive for efficient Kesterite solar cells*, **Nano Energy**, 89B (2021) 106405. https://doi.org/10.1016/j.nanoen.2021.106405
2. NREL chart https://www.nrel.gov/pv/cell-efficiency
3. Schorr, S., G. Gurieva, M. Guc, M. Dimitievska, A. Perez-Rodriguez, V. Izquierdo-Roca, C. Schnohr, J. Kim, W. Jo, J. M. Merino, Point defects, compositional fluctuations, secondary phases in non-stoichiometric kesterites, J. Phys. Energy, 2 (2020) 012002. https://doi.org/10.1088/2515-7655/ab4a25/
4. Schorr S., *The crystal structure of kesterite type compounds: A neutron and X-ray diffraction study*, **Solar Energy Materials and Solar Cells**, 95 (2011) 1482. https://doi.org/10.1016/j.solmat.2011.01.002
5. Gurieva G., Valle Rios L.E., Franz A., Whitfield P., Schorr S., *Intrinsic point defects in off-stoichiometric $Cu_2ZnSnSe_4$: A neutron diffraction study*, **Journal of Applied Physics**, 123 (2018) 161519. https://doi.org/10.1063/1.4997402
6. Park J.S., Kim S., Xie Z., Walsh A., *Point defect engineering in thin-film solar cells*, **Nature Reviews Materials**, 3 (2018) 194–210 https://doi.org/10.1038/s41578-018-0026-7 .

View Article Online
DOI: 10.1039/D6FD00010J

7. Többens D. M., Gurieva G., Levcenko S., Unold T., Schorr S., *Temperature dependency of Cu/Zn ordering in CZTSe kesterites determined by anomalous diffraction*, **Physica Status Solidi B**, 253 (2016) 1890–1897. https://doi.org/10.1002/pssb.201600372
8. Schorr S., Gonzalez-Aviles G., *In-situ investigation of the structural phase transition in kesterite*, **Physica Status Solidi A**, 206 (2009) 1054. https://doi.org/10.1002/pssa.200881214
9. Scragg J.J.S., Choubrac L., Lafond A., Ericson T., Platzer-Björkman C., *A low-temperature order–disorder transition in Cu_2ZnSnS_4 thin films*, **Applied Physics Letters**, 104 (2014) 041911 https://doi.org/10.1063/1.4863685
10. Krammer C., Huber C., Zimmermann C., Lang M., Schnabel T., Abzieher T., Ahlswede E., Kalt H., Hetterich M., *Reversible order–disorder related band gap changes in $Cu_2ZnSn(S,Se)_4$ via post-annealing of solar cells measured by electroreflectance*, **Applied Physics Letters**, 105 (2014) 262104.. https://doi.org/10.1063/1.4905351
11. Rey G., Redinger A., Sendler J., Weiss T.P., Thevenin M., Guennou M., El Adib B., Siebentritt S., *The band gap of $Cu_2ZnSnSe_4$: Effect of order–disorder*, **Applied Physics Letters**, 105 (2014) 112106. https://doi.org/10.1063/1.4896315
12. Schorr S., *X-Ray and Neutron Diffraction on Materials for Thin-Film Solar Cells*, in: Abou-Ras D., Kirchartz T., Rau U. (Eds.), **Advanced Characterization Techniques for Thin Film Solar Cells**, Wiley-VCH, 2011, p. 347.
13. Meissner D., Ernits K., Gahr S., Kapitan L., Vetter M., Glatz C., Syed R., *Kesterite based monograin photovoltaics: the ideal solution for sustainable power supply*, **Solar Energy Materials and Solar Cells**, 252 (2023) 112160. https://doi.org/10.1016/j.solmat.2022.112160
14. Mellikov E., Altosaar M., Kauk – Kuusik M., Timmo K., Meissner D., Grossberg M., Krustok J. and Volobujeva O., (2015) Growth of CZTS-Based Monograins and Their Application to Membrane Solar Cells, in: K. Ito (Eds.), Copper Zinc Tin Sulfide-Based Thin-Film Solar Cells, John Wiley & Sons, Ltd., pp. 289-309. https://doi.org/10.1002/9781118437865.ch13
15. Mellikov E., Volobujeva O., Meissner D., Iljina J., Altosaar M., Timmo K., Klavina I., Varema T., Muska K., Kauk M., Krustok J., Raudoja J., Öpik A., Grossberg M., Ganchev M., Bereznev S., Danilson M., *CZTS monograin powders and thin films*, **Advanced Materials Research**, 222 (2011) 8–13. https://doi.org/10.4028/www.scientific.net/AMR.222.8
16. Peharz G., Satzinger V., Pötz S., Oreski G., Dimopoulos T., Edinger S., Hackl W., StarklH., Esfandiari P., Krabb P., Gahr S., Plessing L., Meissner D., Challenges in the industrial production of CZTS monograin solar cells, in: 2017 IEEE 44th Photovoltaic Specialist Conference (PVSC), IEEE, 2017. https://doi.org/10.1109/PVSC.2017.8366265
17. Maalouf A., Okoroafor T., Resalati S., Gahr S., Ernits K., Meissner D., *Environmental performance of kesterite monograin module production in comparison to thin-film technology*, **Solar Energy Materials & Solar Cells**, 251 (2023) 112161. https://doi.org/10.1016/j.solmat.2022.112161
18. Gurieva G., Rotaru V., Ernits K., Siminel N., Manjón-Sanz A., Kirkham M., Perez-Rodriguez A., Guc M., Meissner D., Schorr S., *To grind or not to grind? The influence of mechanical and thermal treatments on the Cu/Zn disorder in $Cu_2ZnSn(S_xSe_{1-x})_4$ monograins*, **Solar Energy Materials and Solar Cells**, 248 (2022) 112009. https://doi.org/10.1016/j.solmat.2022.112009.
19. Gurieva G., Ernits K., Levcenko S., Franz A., Meissner D., Schorr S., *Influence of Cu purity and low-temperature annealing on Cu/Zn disorder and efficiency of CZTSSe monograins*, **Physical Review Materials**, 9 (2025) 075403. https://doi.org/10.1103/37sc-4jmy
20. Larramona G., Choné C., Meissner D., Ernits K., Bras P., Ren Y., Martín-Salinas R., Rodríguez-Villatoro J.L., Vermang B., Brammertz G., *Stability, reliability, upscaling and possible technological applications of kesterite solar cells*, **Journal of Physics: Energy**, 2 (2020) 024009 https://doi.org/10.1088/2515-7655/ab7cee
21. Fischer P., Frey G., Koch M., Konnecke M., Pomjakushin V., Schefer J., Thut R., Schlumpf N., Bürge R., Greuter U., Bondt S., Berruyer E., *High-resolution powder diffractometer HRPT for thermal neutrons at SINQ*, **Physica B: Condensed Matter**, 276–278 (2000) 146–147. https://doi.org/10.1016/S0921-

4526(99)01399-X

22. Fischer P., Schefer J., Keller L., Zaharko O., Pomjakushin V., Sheptyakov D., Aliouane N., Frontzek M., Holm S.L., Lefmann K., *50 years of Swiss neutron diffraction instrumentation*, **Swiss Neutron News**, 42 (2013).
23. Huq A., Kirkham M.J., Peterson P.F., Hodges J.P., Whitfield P., Page K., Huegle T., Iverson E.B., Parizzi A., Rennich G.Q., *POWGEN: rebuild of a third-generation powder diffractometer at the Spallation Neutron Source*, **Journal of Applied Crystallography**, 52 (2019) 1189–1201. https://doi.org/10.1107/S160057671901121X
24. Avdeev M., Hester J.R., *ECHIDNA: a decade of high-resolution neutron powder diffraction at OPAL*, **Journal of Applied Crystallography**, 51 (2018) 1597–1604. https://doi.org/10.1107/S1600576718014048
25. Rietveld H.M., *A profile refinement method for nuclear and magnetic structures*, **Journal of Applied Crystallography**, 2 (1969) 65–71. https://doi.org/10.1107/S0021889869006558
26. Juan Rodriguez-Carvajal and Thierry Roisnel, www.ill.eu/sites/fullprof
27. Schorr S., Höbler H.-J., Tovar M., *A neutron diffraction study of the stannite–kesterite solid solution series*, **European Journal of Mineralogy**, 19 (2007) 65–73. https://doi.org/10.1127/0935-1221/2007/0019-0065
28. S. Schorr and G. Gurieva, (2021) Energy band gap variations in chalcogenide compound semiconductors: influence of crystal structure, structural disorder, and compositional variations, In: S. Schorr and C. Weidenthaler (Eds.), Crystallography in Materials Science: From Structure-Property Relationships to Engineering, Walter de Gruyter GmbH, Berlin/Munich/Boston, pp. 123-151. https://doi.org/10.1515/9783110674910-004
29. Gurieva G., Többens D.M., Levcenco S., Unold T., Schorr S., *Cu/Zn disorder in stoichiometric $Cu_2ZnSn(S_{1-x}Se_x)_4$ semiconductors: A complementary neutron and anomalous X-ray diffraction study*, **Journal of Alloys and Compounds**, 846 (2020) 156304. https://doi.org/10.1016/j.jallcom.2020.156304.
30. Walsh A., Chen S., Wei S.-H., Gong X.-G., *Kesterite thin-film solar cells: Advances in materials modelling of Cu_2ZnSnS_4*, **Advanced Energy Materials**, 2 (2012) 400–409. https://doi.org/10.1002/aenm.201100630

View Online
DOI: 10.1039/D6FD00010J

Tables

Table 1. Overview of the synthesized monograin samples: cation ratios Cu/(Zn+Sn), Zn/Sn and anion ratio S/(S+Se) of the CZTSSe main phase obtained from the WDX analysis, chemical formula, off-stoichiometry type and presence of secondary phases.

sample	Cu/Sn+Zn	Zn/Sn	S/(S+Se)	Secondary phases	Cu	Type	defects [5]
E_01_so	0.931 (1)	1.095 (1)	0.819 (1)	-	$Cu_{1.92}Zn_{1.08}Sn_{0.98}S_{3.28}Se_{0.72}$	A - B	**A**: $V_{Cu}+Zn_{Cu}$ **B**: $2Zn_{Cu}+Zn_{Sn}$ **G**: $Zn_{Sn}+Zn_i$ **L**: $4V_{Cu}+Zn_{Cu}+Sn_{Cu}$
E_02_so	0.932 (1)	1.087 (1)	0.819 (1)	-	$Cu_{1.92}Zn_{1.07}Sn_{0.99}S_{3.28}Se_{0.72}$	A - B	
E_03_so	0.934 (1)	1.084 (1)	0.817 (1)	-	$Cu_{1.92}Zn_{1.07}Sn_{0.99}S_{3.27}Se_{0.73}$	A - B	
B_01_sg	0.947 (1)	1.026 (1)	0.815 (1)	ZnS	$Cu_{1.93}Zn_{1.03}Sn_{1.00}S_{3.26}Se_{0.74}$	A - L	
B_04_og	0.947 (1)	1.014 (1)	0.810 (1)	ZnS	$Cu_{1.92}Zn_{1.02}Sn_{1.01}S_{3.24}Se_{0.76}$	A - L	
A_01_o	0.966 (1)	1.080 (1)	0.805 (1)	-	$Cu_{1.97}Zn_{1.06}Sn_{0.98}S_{3.22}Se_{0.78}$	B - G	
A_06_og	0.974 (1)	1.047 (1)	0.816 (1)	-	$Cu_{1.98}Zn_{1.04}Sn_{0.99}S_{3.26}Se_{0.74}$	A - B	
D_01_o	0.941 (1)	1.070 (1)	0.810 (1)	$ZnS_{0.9}Se_{0.1}$	$Cu_{1.93}Zn_{1.06}Sn_{0.99}S_{3.24}Se_{0.76}$	A - B	
D_02_o	0.944 (1)	1.058 (1)	0.811 (1)	$ZnS_{0.9}Se_{0.1}$	$Cu_{1.93}Zn_{1.05}Sn_{0.99}S_{3.24}Se_{0.76}$	A - B	
D_07_o	0.948 (1)	1.061 (1)	0.810 (1)	-	$Cu_{1.94}Zn_{1.05}Sn_{0.99}S_{3.24}Se_{0.76}$	A - B	
C-01_o	0.923 (1)	1.061 (1)	0.811 (1)	ZnS	$Cu_{1.90}Zn_{1.06}Sn_{1.00}S_{3.24}Se_{0.76}$	A - B	
C-03_sg	0.948 (1)	1.022 (1)	0.813 (1)	ZnS	$Cu_{1.93}Zn_{1.03}Sn_{1.00}S_{3.25}Se_{0.75}$	A - L	
B-02_sg	0.948 (1)	1.029 (1)	0.808 (1)	ZnS	$Cu_{1.93}Zn_{1.03}Sn_{1.00}S_{3.23}Se_{0.77}$	A - L	
A-02_o	0.972 (1)	1.064 (1)	0.803 (1)	-	$Cu_{1.97}Zn_{1.05}Sn_{0.98}S_{3.21}Se_{0.79}$	B - G	
A-03_o	0.968 (1)	1.055 (1)	0.821 (1)	-	$Cu_{1.95}Zn_{1.04}Sn_{0.99}S_{3.28}Se_{0.72}$	A - B	
A-05_om	0.976 (1)	1.036 (1)	0.815 (1)	ZnS	$Cu_{1.97}Zn_{1.03}Sn_{0.99}S_{3.26}Se_{0.74}$	A - B	
A-07_o	0.963 (1)	1.071 (1)	0.814 (1)	$ZnS_{0.9}Se_{0.1}$	$Cu_{1.96}Zn_{1.05}Sn_{0.98}S_{3.26}Se_{0.74}$	A - B	
A-08_o	0.958 (1)	1.073 (1)	0.813 (1)	ZnS	$Cu_{1.95}Zn_{1.06}Sn_{0.98}S_{3.25}Se_{0.75}$	A - B	
A-09_s	0.971 (1)	1.059 (1)	0.811 (1)	$ZnS_{0.9}Se_{0.1}$	$Cu_{1.97}Zn_{1.04}Sn_{0.98}S_{3.24}Se_{0.76}$	A - B	

Table 2. Lattice parameters and site occupancy factors of CZTSSe monograins determined by Rietveld analysis of the neutron diffraction data.

View Article Online
DOI: 10.1039/D6FD00010J

sample	*a*, Å	*c*, Å	SOF Cu 2*a*	SOF Cu 2*c*	SOF Zn 2*d*	Instrument
E_01_so	5.481 (1)	10.934 (2)	0.970 (17)	0.914 (22)	1.135 (26)	POWGEN
E_02_so	5.481 (1)	10.934 (2)	0.952 (18)	0.957 (26)	1.112 (27)	POWGEN
E_03_so	5.481 (1)	10.934 (2)	0.925 (17)	0.985 (22)	1.119 (24)	POWGEN
B_01_sg	5.482 (1)	10.933 (2)	0.991 (20)	0.892 (26)	1.177 (28)	POWGEN
B_04_og	5.482 (1)	10.934 (2)	0.967 (19)	0.919 (22)	1.148 (27)	POWGEN
A_01_o	5.482 (1)	10.936 (2)	1.004 (20)	0.904 (22)	1.159 (19)	HRPT
A_06_og	5.481 (1)	10.932 (2)	1.010 (22)	0.906 (36)	1.158 (36)	HRPT
D_01_o	5.487 (1)	10.945 (2)	0.922 (21)	0.937 (26)	1.141 (21)	HRPT
D_02_o	5.487 (1)	10.946 (2)	0.915 (25)	0.960 (26)	1.120 (21)	HRPT
D_07_o	5.487 (1)	10.945 (2)	0.985 (20)	0.913 (31)	1.133 (30)	HRPT
C-01_o	5.487 (1)	10.945 (2)	0.944 (21)	0.919 (43)	1.169 (43)	HRPT
C-03_sg	5.487 (1)	10.944 (2)	0.964 (26)	0.903 (46)	1.180 (46)	HRPT
B-02_sg	5.487 (1)	10.945 (2)	1.000 (26)	0.917 (43)	1.135 (43)	HRPT
A-02_o	5.486 (1)	10.945 (2)	0.989 (20)	0.922 (43)	1.181 (43)	HRPT
A-03_o	5.487 (1)	10.943 (2)	1.006 (18)	0.893 (32)	1.132 (34)	HRPT
A-05_om	5.487 (1)	10.931 (2)	0.969 (26)	0.921 (22)	1.079 (22)	Echidna
A-07_o	5.486 (1)	10.947 (2)	0.983 (23)	0.891 (43)	1.150 (43)	HRPT
A-08_o	5.482 (1)	10.935 (2)	0.945 (29)	0.919 (32)	1.035 (32)	Echidna
A-09_s	5.482 (1)	10.935 (2)	0.972 (29)	0.864 (32)	1.058 (32)	Echidna

Table 3. Intrinsic point defects: concentration of as off-stoichiometry related defects as well as Cu/Zn disorder (as fractions of the respective site) in CZTSSe monograins.

View Article Online
DOI: 10.1039/D6FD00010J

sample	A-B											
	V_{Cu}	error	Zn_{Cu}	error +	error -	Zn_{Sn}	error	Cu/Zn	error +	error -	Q	error
E_01_so	0.024	0.004	0.059	0.011	0.004	0.017	0.0001	0.350	0.060	0.019	0.300	0.063
E_02_so	0.027	0.003	0.056	0.011	0.006	0.015	0.0001	0.240	0.072	0.001	0.520	0.07
E_03_so	0.027	0.011	0.054	0.016	0.003	0.014	0.0001	0.300	0.063	0.024	0.400	0.06
A_06_og	0.003	0.001	0.025	0.009	0.003	0.011	0.0001	0.400	0.123	0.058	0.200	0.13
D_01_o	0.026	0.004	0.047	0.009	0.008	0.011	0.0001	0.400	0.042	0.053	0.200	0.06
D_02_o	0.028	0.006	0.043	0.009	0.008	0.007	0.0001	0.340	0.036	0.044	0.320	0.05
D_07_o	0.024	0.006	0.041	0.013	0.005	0.010	0.0001	0.350	0.074	0.044	0.300	0.08
C-01_o	0.055	0.050	0.055	0.021	0.008	0.003	0.0001	0.400	0.155	0.039	0.200	0.16
A-03_o	0.005	0.001	0.029	0.007	0.004	0.012	0.0001	0.390	0.057	0.092	0.220	0.10
A-05_om	0.004	0.001	0.023	0.001	0.007	0.005	0.0001	0.250	0.016	0.046	0.500	0.04
A-07_o	0.003	0.001	0.036	0.006	0.007	0.017	0.0001	0.410	0.085	0.072	0.180	0.11
A-08_o	0.006	0.003	0.040	0.001	0.022	0.016	0.0001	0.180	0.002	0.058	0.640	0.05
A-09_s	0.001	0.001	0.029	0.002	0.015	0.015	0.0001	0.300	0.018	0.151	0.400	0.15
	A-L											
	V	**Error**	Zn_{Cu}	**error +**	**error -**	Sn_{Cu}	**error**	**Cu/Zn**	**error +**	**error -**	**Q**	**error**
B_01_sg	0.030	0.010	0.035	0.011	0.001	0.004	0.0001	0.425	0.143	0.001	0.145	0.14
B_04_og	0.045	0.012	0.022	0.006	0.001	0.008	0.0021	0.350	0.086	0.006	0.300	0.08
C-03_sg	0.042	0.012	0.027	0.011	0.003	0.027	0.0015	0.450	0.157	0.062	0.100	0.16
B-02_sg	0.039	0.001	0.042	0.019	0.003	0.002	0.0008	0.348	0.126	0.043	0.293	0.13
	B-G											
	Zn_i	**Error**	Zn_{Cu}	**error +**	**error -**	Zn_{Sn}	**error**	**Cu/Zn**	**error +**	**error -**	**Q**	**erro**
A_01_o	0.005	0.001	0.032	0.008	0.002	0.021	0.0001	0.420	0.067	0.027	0.160	0.07
A-02_o	0.002	0.001	0.027	0.008	0.001	0.017	0.0001	0.440	0.127	0.012	0.120	0.12

Table 4 Optical bangap energy of CZTSSe monograins obtained from diffuse reflectance, solar cell efficiency and stability as defined in [20].

View Article Online
DOI: 10.1039/D6FD00010J

	E_g, eV	Efficiency, % [20]	Stability [13]
E_01_so	1.236 (23)	6.09	0.13
E_02_so	1.242 (22)	6.25	0.14
E_03_so	1.232 (24)	6.02	0.18
B_01_sg	1.207 (28)	6.78	0.92
B_04_og	1.375 (27)	6.76	0.96
A_01_o	-	6.79	0.98
A_06_og	1.217 (29)	6.24	1.00
D_01_o	1.241 (31)	6.17	0.28
D_02_o	1.217 (23)	6.96	0.28
D_07_o	1.242 (27)	6.54	0.64
C-01_o	1.213 (49)	7.07	0.66
C-03_sg	1.194 (67)	6.19	0.72
B-02_sg	1.20 (40)	6.76	0.93
A-02_o	1.215 (51)	6.09	0.99
A-03_o	1.222 (59)	6.13	1.00
A-05_om	1.286 (4)	6.43	1.00
A-07_o	1.246 (39)	6.58	1.00
A-08_o	1.249 (16)	6.56	1.00
A-09_s	1.208 (15)	6.59	1.00

Figures

View Article Online
DOI: 10.1039/D6FD00010J

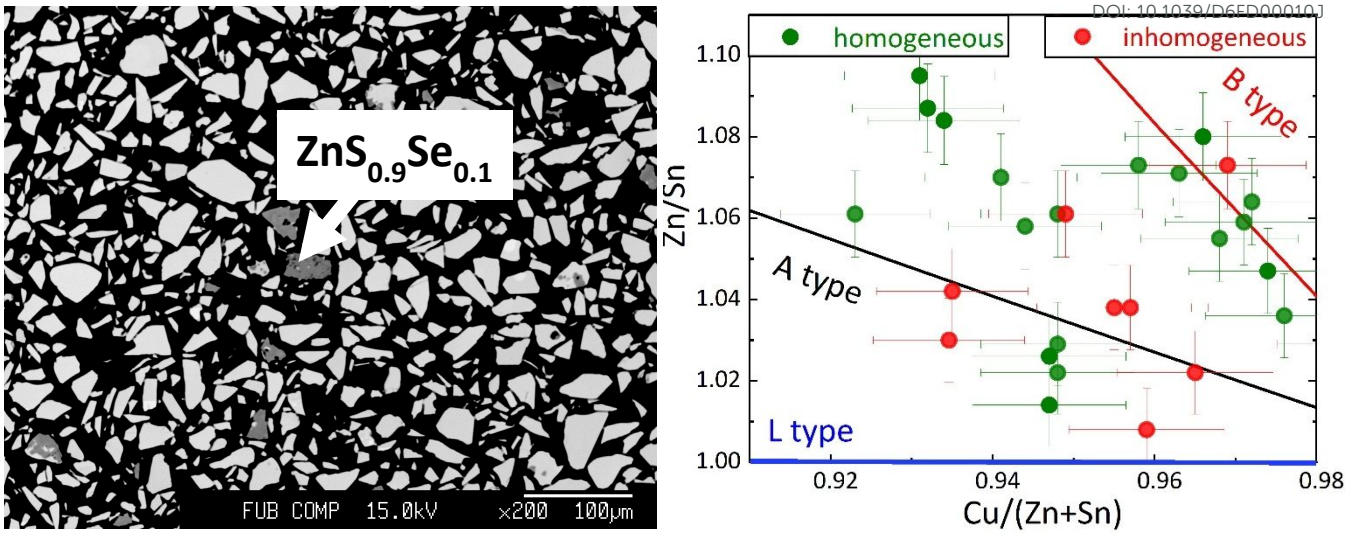

Figure 1 (left)Back-scatter electron (BSE) micrograph of a representative sample showing CZTSSe grains (lighter grey) embedded in epoxy (black) with highlighted $ZnS_{0.9}Se_{0.1}$ secondary phase (darker grey); (right) cation ratio plot showing all 27 monograins. The inhomogeneous samples, excluded from the further study are shown in red.

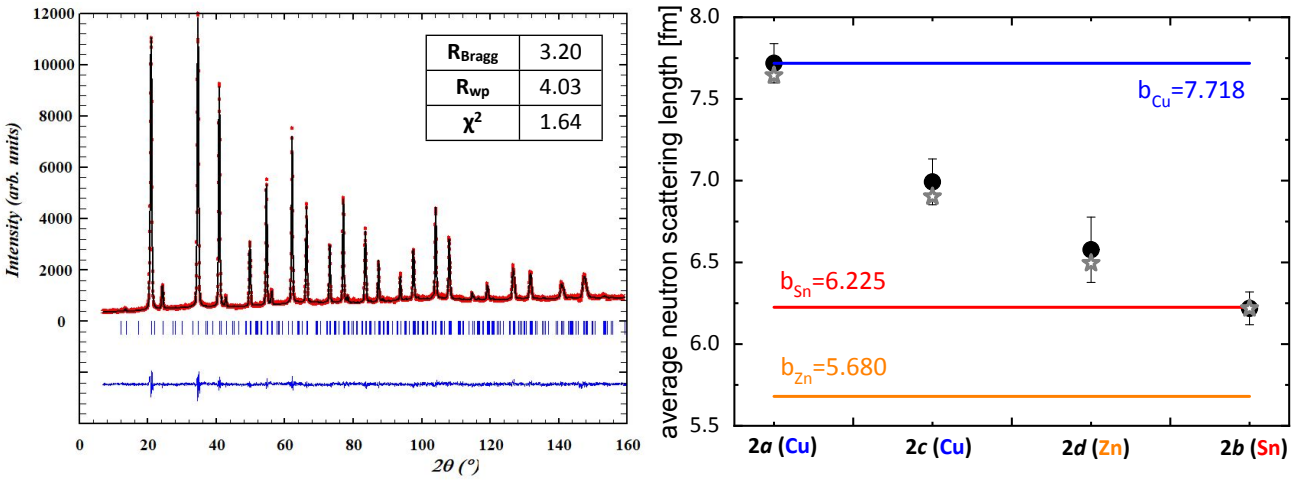

Figure 2 (left) Rietveld refinement of the neutron diffraction data of the $Cu_{1.98}Zn_{1.04}Sn_{0.99}S_{3.26}Se_{0.74}$ (NPD performed at HRPT, SINQ, PSI, Switzerland) where the red dots are experimental data, the black line is the obtained fit, the blue ticks are the Bragg peak positions of the kesterite type structure, and the blue line is the difference between the experimental and calculated data; (right) Average neutron scattering length $\bar{b}$ of the cation sites 2*a*, 2*c*, 2*d* and 2*b* for $Cu_{1.98}Zn_{1.04}Sn_{0.99}S_{3.26}Se_{0.74}$ monograins, (full symbols – experimental values; star – calculated values from the best fitting cation distribution model; lines – pure elements).

View Article Online
DOI: 10.1039/D6FD00010J

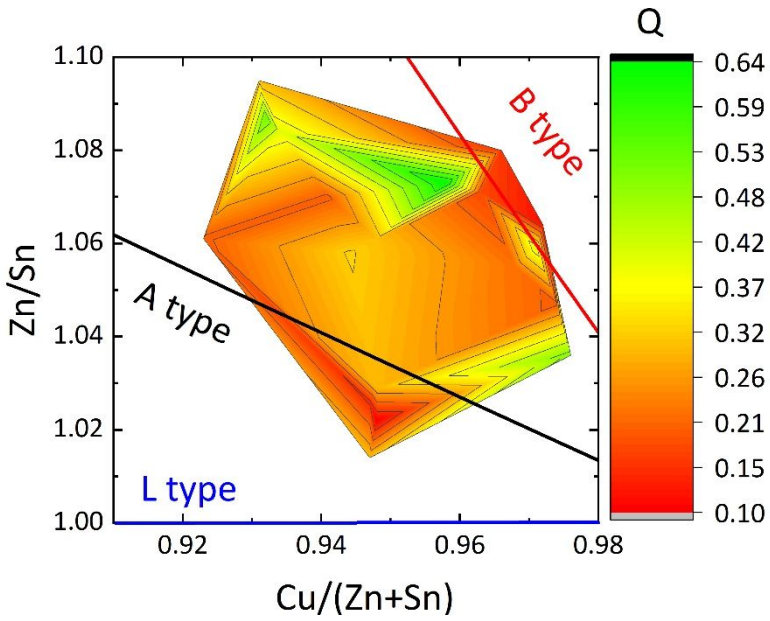

Figure 3 Order parameter Q of the Cu/Zn disorder calculated from the Cu and Zn distribution on the Wyckoff positions 2c and 2d (according to eq. 2) for CZTSSe monograins mapped on the cation ratio plot.

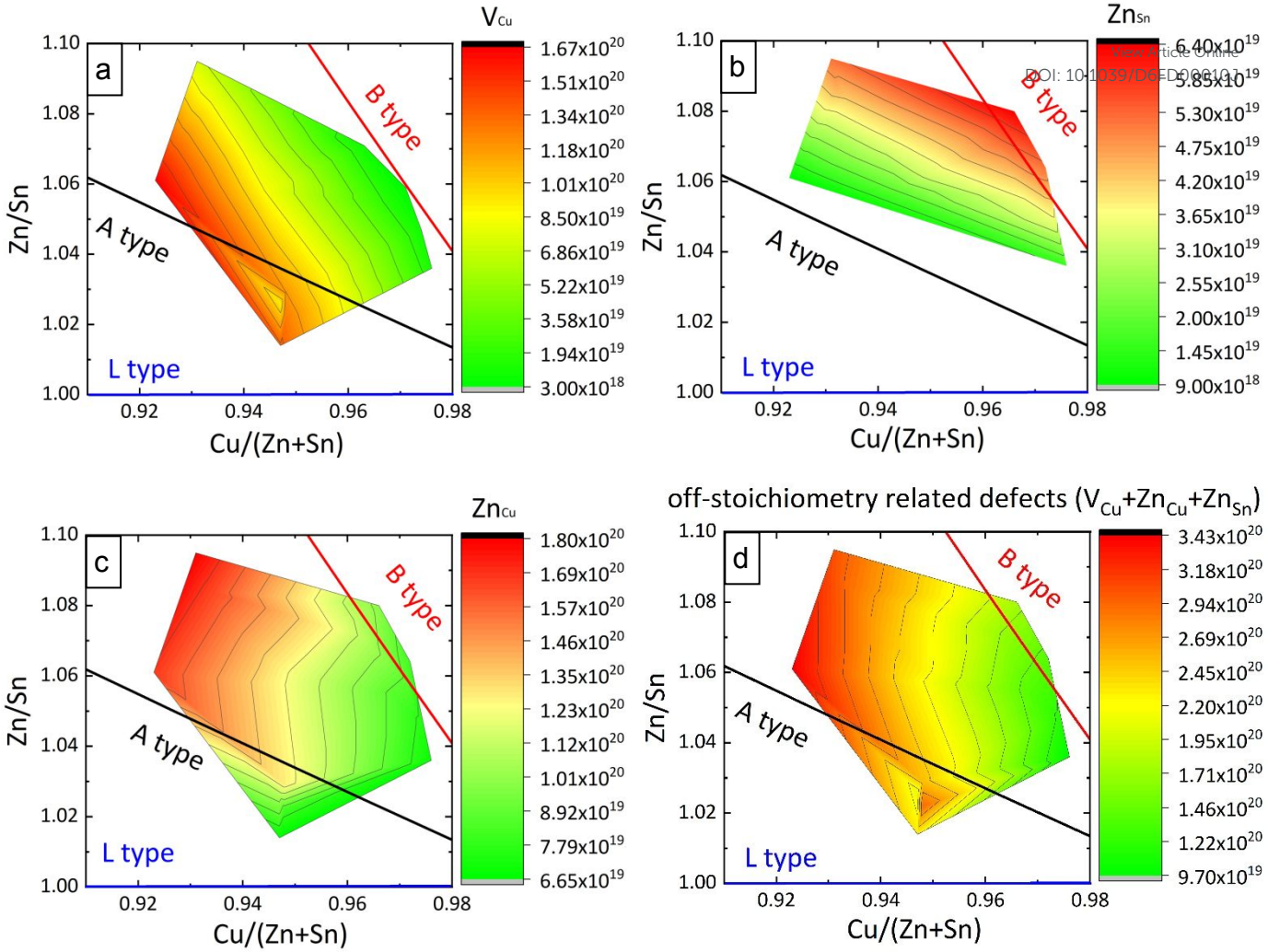

Figure 4 Concentration (defects/cm^3) of the intrinsic point defects V_{Cu} Zn_{Cu}, Zn_{Sn} and a total sum of point defects related to the off-stoichiometric composition derived from the cation distribution model established by the average neutron scattering length analysis of the neutron diffraction data.

View Article Online
DOI: 10.1039/D6FD00010J

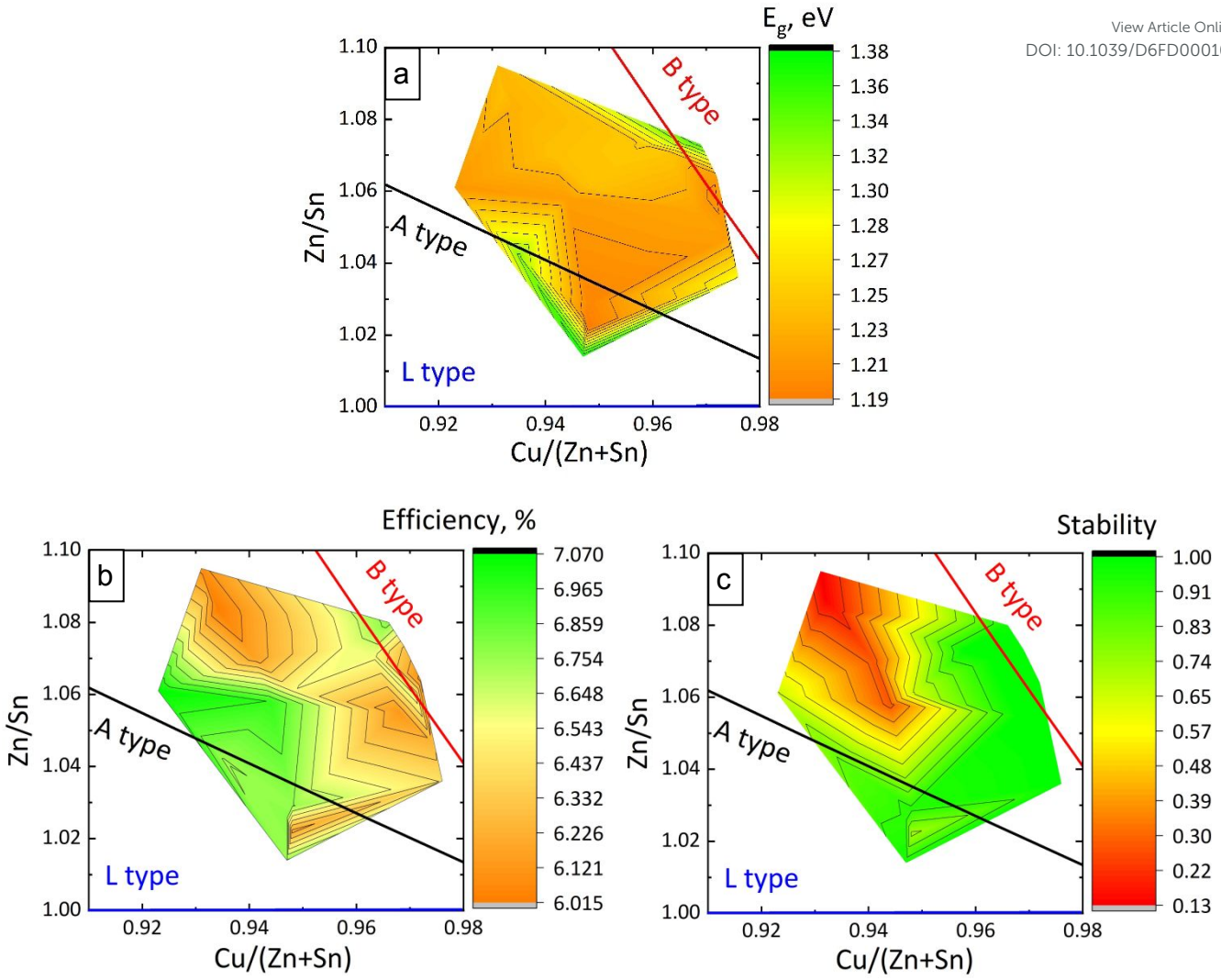

Figure 5 The band gap energy, efficiency and stability of corresponding monograin-layer based solar cells using CZTSSe monograins with S/(S+Se)=0.8.

The data cannot be made publicly available upon publication because the cost of preparing, depositing and hosting the data would be prohibitive within the terms of this research project. The data that support the findings of this study are available upon reasonable request from the authors.

View Article Online
DOI: 10.1039/D6FD00010J